Crystal structures of porcine STING^{CBD}–CDN complexes reveal the mechanism of ligand recognition and discrimination of STING proteins

Received for publication, January 2, 2019, and in revised form, June 2, 2019 Published, Papers in Press, June 5, 2019, DOI 10.1074/jbc.RA119.007367

Xiaoyan Cong[‡§1], Zenglin Yuan[‡1], Yijun Du[§], Bo Wu[¶], Defen Lu[‡], Xiangju Wu[§], Youjia Zhang[¶], Feng Li[‖], Bin Wei[**], Jun Li[§], Jiaqiang Wu[§], Sujuan Xu[‡], Jinbao Wang[†‡], Jing Qi[§2], Guijun Shang[‡3], and Lichuan Gu[‡4]

From the [‡]State Key Laboratory of Microbial Technology, Shandong University, Jinan 250100, China, the [§]Shandong Key Laboratory of Animal Disease Control and Breeding, Institute of Animal Science and Veterinary Medicine, Shandong Academy of Agricultural Sciences, Sangyuan Rd. No. 8, Jinan 250100, China, the [¶]High Magnetic Field Laboratory, Key Laboratory of High Magnetic Field and Ion Beam Physical Biology, Hefei Institutes of Physical Science, Chinese Academy of Sciences, Hefei 230026, Anhui, China, the [‖]Department of Biology and Microbiology, Department of Veterinary and Biomedical Sciences, South Dakota State University, Brookings, South Dakota 57007, and the [**]Shandong Asia-Pacific Highharve Organisms Science and Technology Co., Ltd., No. 1 Jinneng Rd., Qihe, Shandong 251100, China

Edited by Wolfgang Peti

The cyclic dinucleotide (CDN)-stimulator of interferon genes (STING) pathway plays an important role in the detection of viral and bacterial pathogens in animals. Previous studies have shown that the metazoan second messenger cyclic [G(2′,5′)pA(3′,5′)p] (2′,3′-cGAMP) generated by cyclic GMP-AMP synthase cGAS binds STING with high affinity compared with bacterial CDNs such as c-di-GMP, c-di-AMP, and 3′,3′-cGAMP. Despite recent progress indicating that the CDN-binding domain (CBD) of dimeric STING binds asymmetric 2′,3′-cGAMP preferentially over symmetric 3′,3′-CDNs, it remains an open question whether STING molecules, such as human STING, adopt a symmetric dimeric conformation to efficiently engage its asymmetric ligand. Here, structural studies of the CBD from porcine STING (STING^{CBD}) in complex with CDNs at 1.76–2.6 Å resolution revealed that porcine STING^{CBD}, unlike its human and mouse counterparts, can adopt an asymmetric ligand-binding pocket to accommodate the CDNs. We observed that the extensive interactions and shape complementarity between asymmetric 2′,3′-cGAMP and the ligand-binding pocket make it the most preferred ligand for porcine STING and that geometry constraints limit the binding between symmetric 3′,3′-CDN and porcine STING. The ligand-discrimination mechanism of porcine STING observed here expands our understanding of how the CDN–STING pathway is activated and of its role in antiviral defense.

This work was supported by National Natural Science Foundation of China Grants 31470732 (to L. G.), 31502051 (to X. C.), 31672609 (to J. Q.) and 21673244 (to Bo. W.) and the National Key Research and Development Program of China Grant 2016YFD0501505 (to Y. D.). The authors declare that they have no conflicts of interest with the contents of this article.
This article contains Figs. S1 and S2 and Table S1.
The atomic coordinates and structure factors (codes 6A03, 6A04, 6A05, 6A06, and 6IYF) have been deposited in the Protein Data Bank (http://wwpdb.org/).

[†] Deceased September 25, 2018.
[1] Both authors contributed equally to this work.
[2] To whom correspondence may be addressed. E-mail: qj-happy2008@163.com.
[3] To whom correspondence may be addressed. E-mail: gjshang@gmail.com.
[4] To whom correspondence may be addressed. E-mail: lcgu@sdu.edu.cn.

The innate immunity system forms the first line of defense against bacterial and viral infections through pattern recognition receptors (PRRs)[5] that detect pathogen-associated molecular patterns (PAMPs) and damage-associated molecular patterns (DAMPs) (1–4). DNAs in the cytosol originating from a bacterial or viral invasion are PAMPs that are recognized by the cytosolic double-strand DNA (dsDNA)-sensing pathways (5). A major cytosolic DNA sensor is cyclic GMP-AMP (cGAS), which synthesizes cyclic [G(2′,5′)pA(3′,5′)p] (2′,3′-cGAMP) upon activation by binding of dsDNA (6). Numerous studies have established that cGAMP functions as the second messenger to bind and activate the endoplasmic reticulum (ER)-located stimulator of interferon genes (STING) (also known as MITA (7, 8), MPYS (9), ERIS (10), and TMEM173 (11)). Ligand-activated STING is quickly translocated from ER to the ER–Golgi intermediate compartment to form punctate structures (12–14). STING uses its C-terminal tail to recruit and activate the TBK1 kinase, which phosphorylates the transcription factor IRF3 (15, 16). Phosphorylated IRF3 becomes an active dimer and then enters the nucleus to induce the expression of type I IFNs, which trigger the host antiviral action.

STING also functions as the direct PRR for other CDNs (17), such as c-di-GMP, c-di-AMP, and 3′,3′-cGAMP, which were first found in bacteria, having important roles in biofilm formation, motility, and virulence (18, 19). The cGAS product 2′,3′-cGAMP is unique in that it not only has two different purine moieties (guanine and adenine) but also contains mixed phosphodiester linkages in which the hydroxyl group of ribose in guanosine was connected at 2′- and 5′-position. In contrast, ribose moieties in all the bacterial CDNs are connected at 3′-

[5] The abbreviations used are: PRR, pattern recognition receptor; PAMP, pathogen-associated molecular pattern; cGAS, cyclic GMP-AMP synthase; PDB, Protein Data Bank; MST, microscale thermophoresis; CDN, cyclic dinucleotide; CBD, CDN-binding domain; STING, stimulator of interferon genes; ER, endoplasmic reticulum; BisTris, 2-[bis(2-hydroxyethyl)-amino]-2-(hydroxymethyl)propane-1,3-diol; PAM, Porcine alveolar macrophage; IFN, interferon.

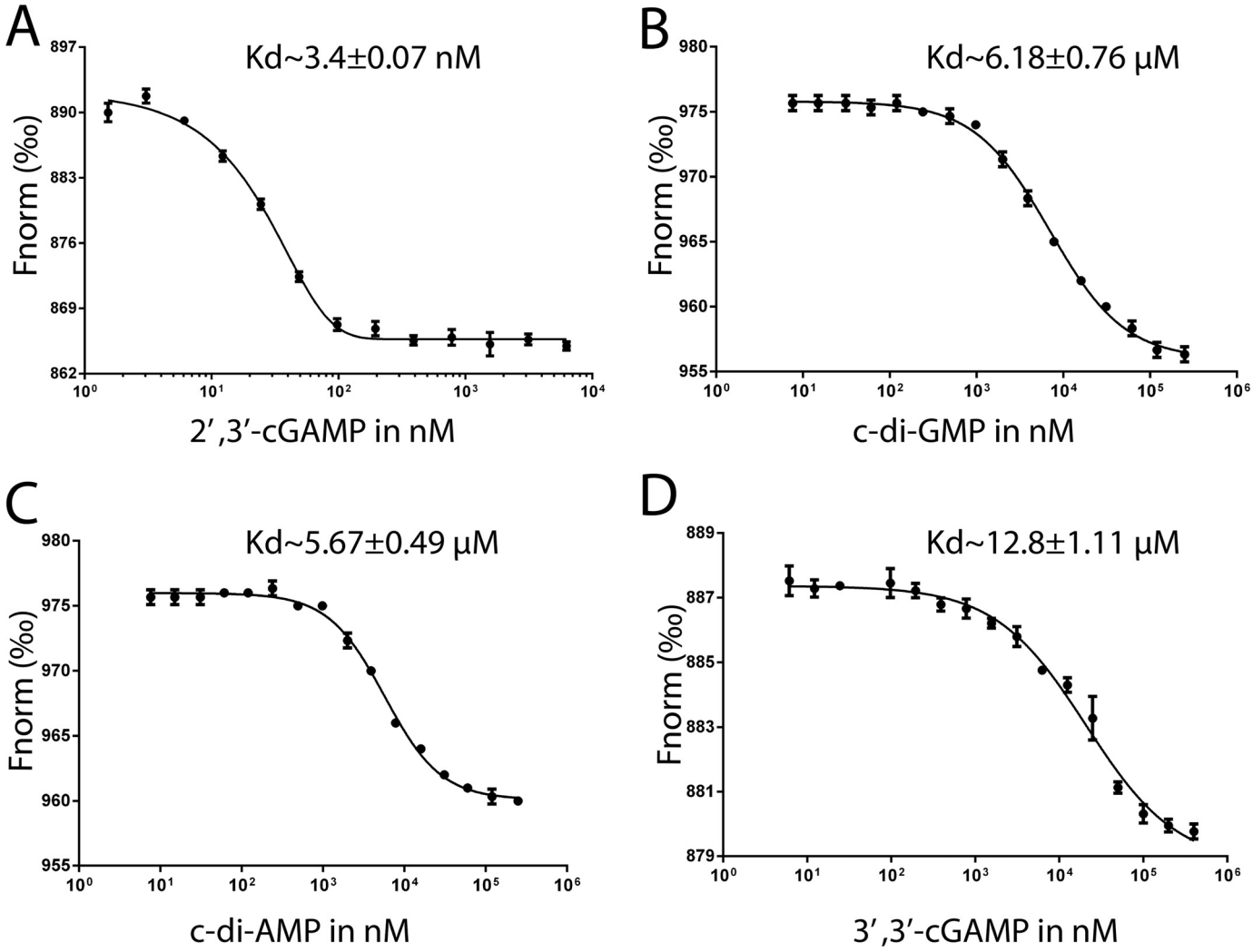

Figure 1. MST assays for quantification of binding between porcine STING^{CBD} protein and four CDNs. The normalized change in the fluorescence of the labeled porcine STING^{CBD} protein was plotted against the CDN concentration. The experiments were performed in triplicate. Mean values ± S.D. ($n = 3$) are shown. *A*, 2′,3′-cGAMP. *B*, c-di-GMP. *C*, c-di-AMP. *D*, 3′,3′-cGAMP.

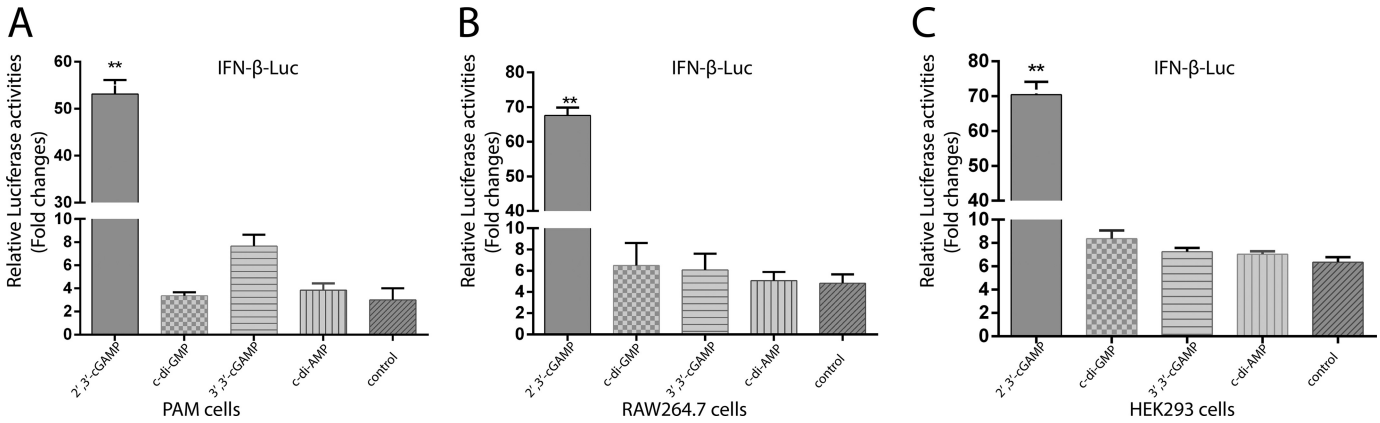

Figure 2. Cell-based luciferase assay of STING in response to CDNs. Cells were transfected with 0.5 μg of IFN-β promoter along with 0.25 μg of pRL-TK. After 18 h of transfection, PAM cells and RAW264.7 cells were incubated with 60 μM CDNs, whereas HEK293 cells were transfected with 60 μM CDNs by using lipo3000. Luciferase reporter assay was performed after an additional 24-h incubation. Values stand for the mean average of triplicate experiments. *Error bars* indicate S.D. *A*, luciferase reporter assay for PAM cells expressing endogenous porcine STING stimulated by CDNs. *B*, luciferase reporter assay for RAW264.7 cells expressing endogenous mouse STING stimulated by CDNs. *C*, luciferase reporter assay for HEK293 cells expressing endogenous human STING stimulated by CDNs.

and 5′-positions. 2′,3′-cGAMP as the endogenous ligand has been shown previously to have higher binding affinity for STING than the bacterial second messengers (20, 21).

The STING protein consists of four transmembrane helices in the N terminus that is followed by the cytosolic CDN-binding domain (CBD). A flexible tail at the C terminus of STING is

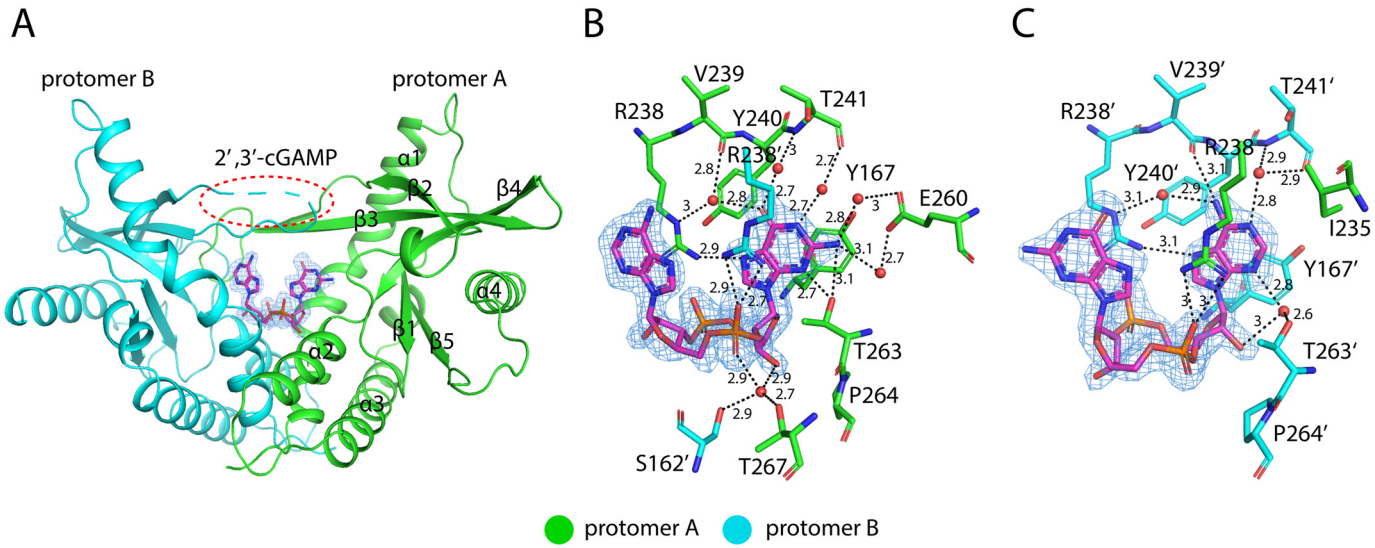

Figure 3. Structure of porcine STING^{CBD} in complex with 2′,3′-cGAMP. Protomers A and B are colored *green* and *cyan*, respectively. The *black dashed line* represents the hydrogen bond formed between ligand and protein. The values indicate the length of hydrogen bond with the unit of Å. The waters are shown as *red sphere*. The ligand is shown as a *stick* model colored in *magenta*. The simulated annealing omit $F_o - F_c$ electron-density map for 2′,3′-cGAMP (*blue mesh*) is contoured at 3 σ. *A*, overall structure of porcine STING^{CBD}–2′,3′-cGAMP complex (side view). The *red dashed circle* shows the disordered lid region in protomer B. *B*, detailed interactions between GMP(2′,5′) moiety of 2′,3′-cGAMP and G site of STING protein. *C*, detailed interactions between AMP(3′,5′) moiety of 2′,3′-cGAMP and A site of STING protein.

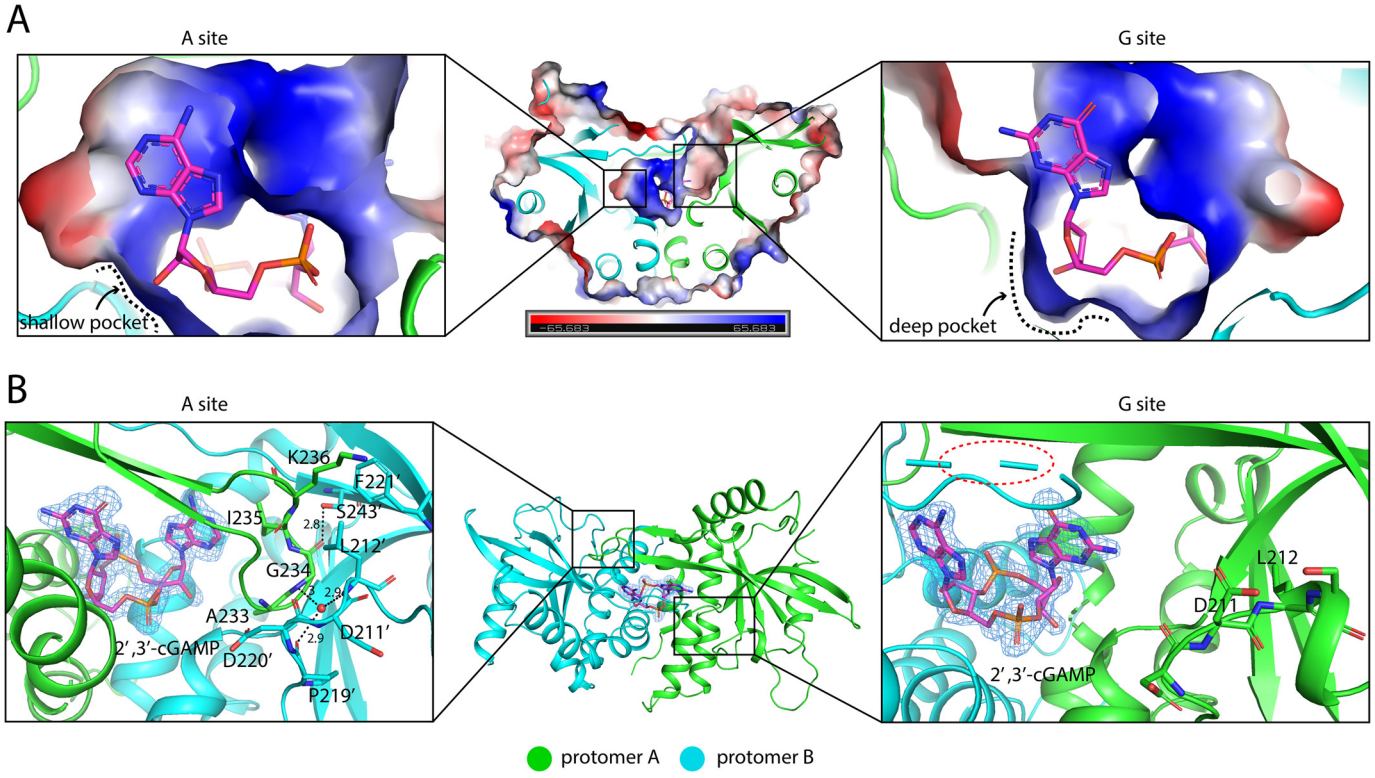

Figure 4. Asymmetric ligand-binding pocket in porcine STING^{CBD}. Protomer A and B are colored *green* and *cyan*, respectively. 2′,3′-cGAMP is shown as a *magenta stick*. *A*, cross-section of 2′,3′-cGAMP–binding pocket in porcine STING^{CBD}. *Left panel* shows the complete A site, and *right panel* shows the incomplete G site. Electrostatic potential is shown. *B, left panel* shows the interactions between hairpin tip of protomer A and protomer B. The water molecule is shown as a *red sphere*. The *black dashed lines* represent the hydrogen bond, and the values show the length of hydrogen bond with the unit of Å. The simulated annealing omit $F_o - F_c$ electron-density map for 2′,3′-cGAMP (*blue mesh*) is contoured at 3 σ. *Middle panel* shows the top view of porcine STING-2′,3′–cGAMP complex. *Right panel* shows the interaction between disordered hairpin of protomer B and protomer A.

important for recruiting and activating TBK1 and IRF3. In the past few years, a myriad of apo-STING and STING–CDNs complex structures from different species has been determined, revealing a dimeric architecture that forms the CDN-binding pocket between the two protomers (22). In the apo-form, the angle between two protomers is relatively large, and the ligand-binding pocket is open. Ligand binding induces conformational changes characterized by a reduced angle between the two protomers and the closure of the "lid" β-strand that encloses the ligand in the deep pocket formed between the two

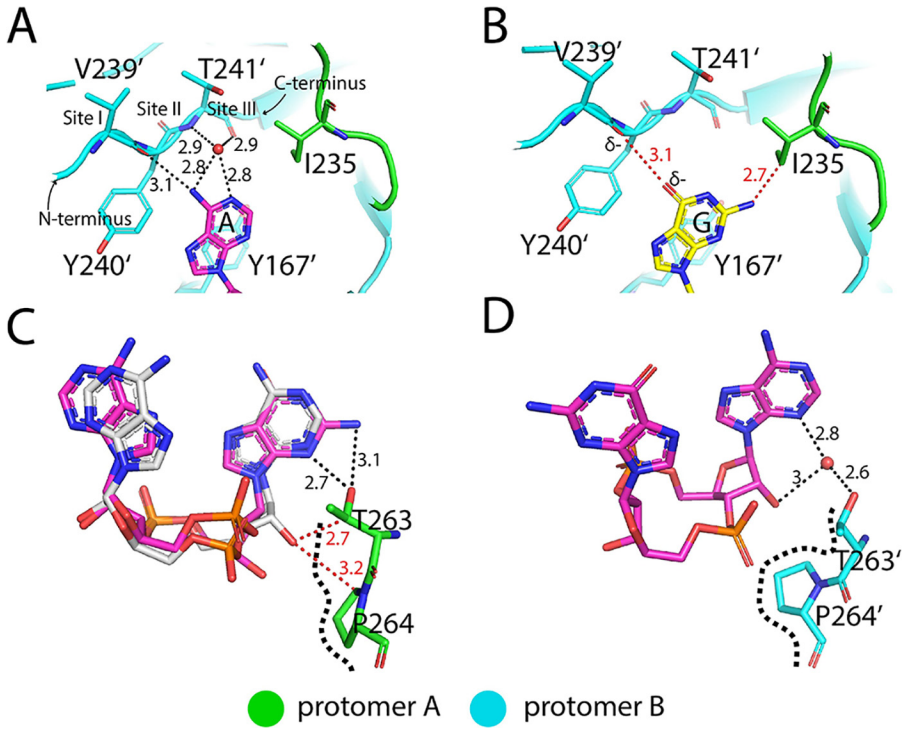

Figure 5. Recognition modes of AMP(3′,5′) and GMP(2′,5′) moieties by porcine STING^{CBD}. The *black dashed lines* represent the hydrogen bond, and the values show the length of hydrogen bond with the unit of Å. The *red dashed line* represents the repulsive van der Waals contact (bad contact or bump), and the values show the distance between nonhydrogen-bonding atoms. The *black dashed curve* represents the boundary of TP motif. *A,* adenine-binding pocket in A site. *B,* guanine was modeled into adenine-binding pocket, and the steric clashes will limit its binding. *C,* sugar edge of guanosine with 2′,5′-phosphodiester bond linkage is recognized by TP motif in G site, whereas the sugar edge of adenosine with 3′,5′ phosphodiester bond linkage will generate steric clashes. c-di-AMP and 2′,3′-cGAMP are shown as sticks colored in *silver* and *magenta*, respectively. *D,* recognition of sugar edge of adenosine with 3′,5′-phosphodiester bond linkage by TP motif in A site. The water is shown as a *red sphere*.

protomers. Recently, the full-length STING was solved by the cryo-EM method (23). It reveals that ligand binding not only induces these conformational changes mentioned above but results in the cytosolic domain half-turn rotation relative to the transmembrane region as well, which adds another layer of regulation of STING signaling.

Until now, all the structures of STING CBD adopt a symmetric dimeric conformation, which is intriguing considering that the asymmetric ligand 2′,3′-cGAMP shows the highest binding affinity. The mechanistic basis for ligand discrimination therefore remains elusive. Here, we determined the CBD of porcine STING complex with four CDNs: 2′,3′-cGAMP; 3′,3′-cGAMP; c-di-GMP; and c-di-AMP. Surprisingly, we found that porcine STING adopts an asymmetric conformation to bind the CDNs. Our analyses of this asymmetric conformation led to a mechanism for ligand recognition and discrimination of STING.

Results

High-affinity binding of porcine STING for 2′,3′-cGAMP

The binding affinities of natural CDNs and various isomers for STING from other species have been extensively studied in the past few years (17, 20, 21, 24–32). These studies show that, in general, the order of binding affinity for natural CDNs is 2′,3′-cGAMP > 3′,3′-cGAMP ≈ c-di-GMP > c-di-AMP. Here, we used the microscale thermophoresis (MST) assay to measure the binding affinity between porcine STING and CDNs. The results show that the binding affinity for 2′,3′-cGAMP with the dissociation constant (K_d) of 3.4 nM (Fig. 1*A*) is comparable with those reported previously for STING from human (4.59 nM) and sea anemone (<1 nM) (21, 31) but is substantially higher than those in mouse and rat STING (submicromolar level, 0.18 and 0.12 μM) (20, 30). The binding affinities of porcine STING for c-di-GMP and c-di-AMP are similar (~6 μM) (Fig. 1, *B* and *C*), which are lower than their human counterpart (21). Furthermore, the binding affinity of porcine STING for 3′,3′-cGAMP ligand is the lowest with a K_d of 12.8 μM in our MST assay (Fig. 1*D*). These results show that, like STING from other species, porcine STING binds the endogenous ligand 2′,3′-cGAMP with the highest binding affinity.

Strong activation of porcine STING by 2′,3′-cGAMP

We then examined whether 2′,3′-cGAMP functions as a potent inducer for IFN-β in porcine immune cells. The IFN-β promoter along with the luciferase reporter gene were transfected into porcine alveolar macrophage (PAM) cells, which have endogenous porcine STING expression. Cells were treated with equal concentrations of CDNs. Fig. 2*A* shows that the 2′,3′-cGAMP stimulated the highest level of IFN-β promoter activity, which is consistent with the results obtained by using mouse and human STING (Fig. 2, *B* and *C*). These results correlate well with the *in vitro* ligand-binding assays, thereby suggesting that 2′,3′-cGAMP is the preferred ligand for porcine STING, as well as human and mouse STING.

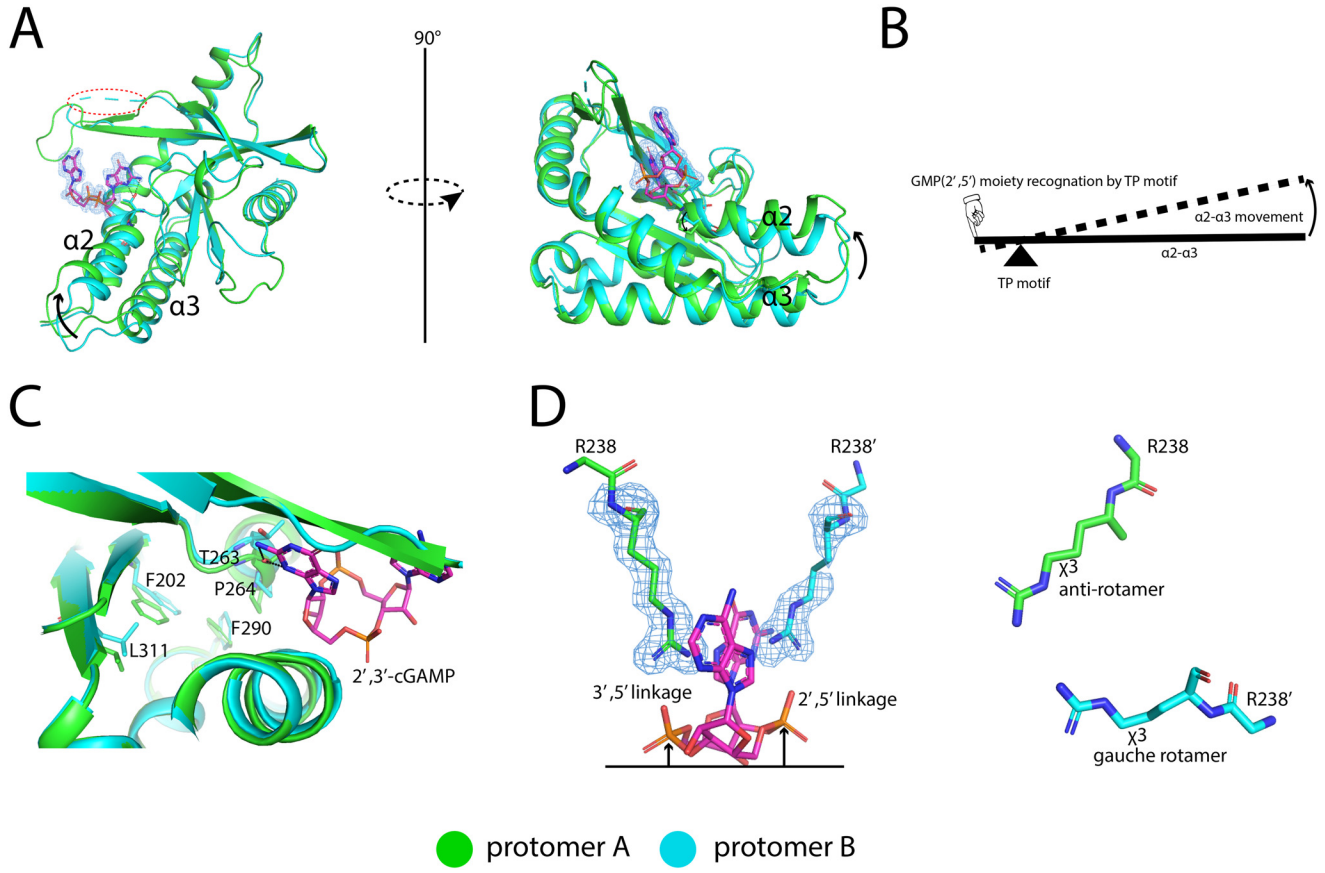

Figure 6. Structural comparison between two protomers in porcine STING^{CBD}–2′,3′-cGAMP complex. 2′,3′-cGAMP is shown with stick colored in *magenta*. The simulated annealing omit $F_o - F_c$ electron-density map for 2′,3′-cGAMP and R238 (blue mesh) is contoured at 3 σ. *A.* superimposition of protomer A and protomer B. The *arrow* indicates the tilt of α2–α3 in protomer A relative to it in protomer B. The *red dashed oval* shows the disordered lid region in protomer B. *B,* working model of the conformational changes of α2–α3 induced by GMP(2′,5′) moiety recognition. *C,* hydrophobic core difference between protomer A and protomer B. *D,* Arg-238 adopts different rotamer in protomer A and protomer B.

Overall structure of porcine STING^{CBD}–2′,3′-cGAMP complex

The structure of porcine STING^{CBD}–2′,3′-cGAMP complex was determined at 1.8 Å resolution. The asymmetric unit contains two STING^{CBD} molecules (protomer A and B) that form the dimer as seen in previous structures of STING^{CBD} from other species (Fig. 3*A*). All residues except residues 228–236 located at the lid region of protomer B are modeled. Porcine STING^{CBD} adopts the same $\alpha + \beta$-fold as STING from other species (22). The individual protomers make extensive interactions with each other through the α1, α2, α3, and central β-sheet region, which forms a deep U-shaped cleft. The 2′,3′-cGAMP ligand is located at the cleft using its purines pointing upward and the ribose ring sticking in the downward position (relevant to the membrane). The base, phosphate, and ribose groups all contribute to binding to STING (Fig. 3, *B* and *C*). The purine rings of 2′,3′-cGAMP stack against Tyr-167 and Arg-238 from two promoters. The phosphate moieties of 2′,3′-cGAMP are recognized by Arg-238 through charge–charge interactions and hydrogen bonds. Arg-238 also forms hydrogen bonds at the Hoogsteen edge of the nucleoside moieties. Beside the stacking interactions, the adenosine and guanosine moieties have different interaction modes with STING. For both, the interactions involve their Watson-Crick, Hoogsteen, and sugar edges (Fig. S1). All the N atoms (except the position-9 amino) and O atom in the purines interact directly or indirectly (water-mediated) with the STING protein (also see details in Table S1). These extensive interactions are consistent with the high binding affinity between ligand and porcine STING^{CBD} as demonstrated in our *in vitro* binding experiment.

Asymmetric ligand-binding pocket in porcine STING

A strikingly distinctive feature of the porcine STING^{CBD}–2′,3′-cGAMP complex is that the two protomers adopt different conformations, resulting in an asymmetric ligand-binding pocket. Consequently, 2′,3′-cGAMP, which is also asymmetric, is held in one well-defined conformation in the ligand-binding pocket (Fig. 4). This unique binding mode is in sharp contrast with that seen in previous structures involving STING proteins from other species (22), where 2′,3′-cGAMP binds the symmetric STING dimer in two alternative modes with the adenosine and guanosine moieties switching positions.

The recognition sites in porcine STING^{CBD} for the adenosine with 3′,5′-phosphodiester bond-linked phosphate (or AMP(3′,5′)) and guanosine with 2′,5′-phosphodiester bond-linked phosphate (or GMP(2′,5′)) moieties show very different conformations. The AMP(3′,5′) moiety recognition pocket (designated as A site) is complete with the ordered lid region and a shallow 3′,5′-phosphodiester linkage sugar edge recognition pocket (Fig. 4*A*, *left panel*). In contrast, the GMP(2′,5′) moiety recognition pocket (designated as G site) is partially

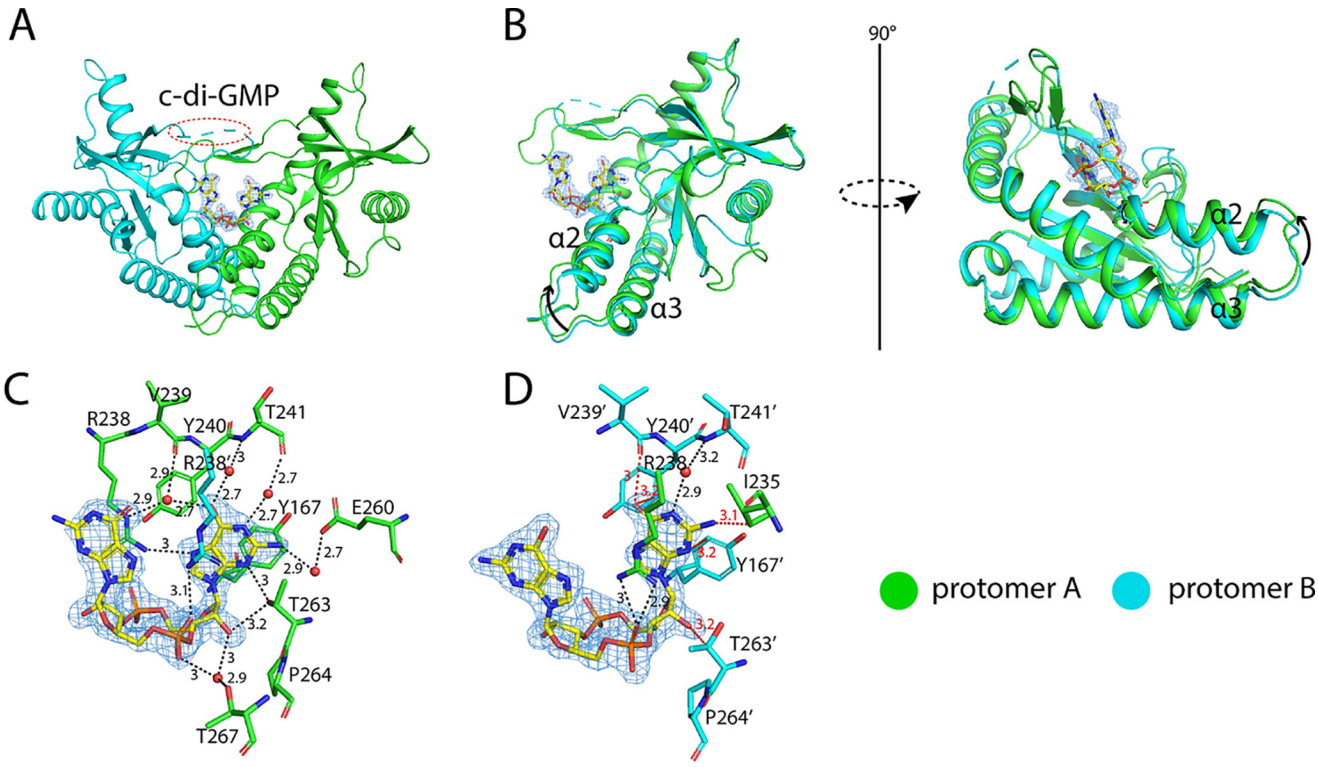

Figure 7. Structure of porcine STING^{CBD} in complex with c-di-GMP. The *black dashed line* represents the hydrogen bond formed between ligand and protein. The values indicate the length of hydrogen bond with the unit of Å. The *red dashed line* represents the repulsive van der Waals contact (bad contact or bump), and the values show the distance between nonhydrogen-bonding atoms. The waters are shown as *red sphere*. The ligand is shown in *stick* model colored in *yellow*. The simulated annealing omit $F_o - F_c$ electron-density map for c-di-GMP (*blue mesh*) is contoured at 3 σ. *A*, overall structure of porcine STING^{CBD}–c-di-GMP complex (side view). The *red dashed circle* shows the disordered lid region in protomer B. *B*, structural comparison between two protomers in porcine STING^{CBD}–c-di-GMP complex. The *arrow* indicates the tilt of α2–α3 in protomer A relative to it in protomer B. *C*, detailed interactions between c-di-GMP and G site of STING protein. *D*, detailed interactions between c-di-GMP and A site of STING protein.

exposed with the β-hairpin tip totally invisible in the density and a deep 2′,5′-phosphodiester linkage sugar edge recognition pocket (Fig. 4*A*, *right panel*).

In the A site, Leu-212 from protomer B flips out and interacts with Phe-221 (protomer B) and Lys-236 (protomer A) through hydrophobic interactions. Leu-212 also buttresses the hairpin tip (Gly-234, Ile-235, and Lys-236) from protomer A, further stabilizing and rigidifying the β-hairpin structure, resulting in the closure of the A site (Fig. 4*B*, *left panel*). Several distinctive features in this pocket of porcine STING appear to underlie its preference for adenosine. The loop region (Val-239, Tyr-240, and Thr-241) and Tyr-167 form an adenine-binding motif, which is found in many adenylate-containing proteins to recognize the adenine ring (Fig. 5*A*, and Fig. S2) (33). Meanwhile, hydrophobic interactions between the aromatic C2 atom of adenine and the aliphatic side chain of Ile-235 further enhance the specific binding of adenine to the pocket. This type of specific adenine recognition mode can also be seen in the double-strand RNA–binding motif such as ADAR2, which uses the side chain of Met to specifically recognize the C2 atom of adenine from RNA (34, 35). However, guanine has an extra exocyclic–amino group at position-2 and carbonyl oxygen at position-6, which are expected to generate van der Waals repulsion (bad contact or bump) with the side chain of Ile-235 and the carbonyl group of Val-239, respectively, disfavoring its binding in this pocket (Fig. 5*B*).

The G site is partially open, as the β-hairpin tip from protomer B is disordered. The loop accommodating the β-hairpin tip adopts a different conformation with the Leu-212 buried in the hydrophobic core of protomer A (Fig. 4*B*, *right panel*). As a result, the guanine moiety of the ligand is partially exposed to solvent. As discussed above, the closed lid as seen for the adenine recognition pocket is not favorable for the binding of the guanine duo to the selectivity of Ile-235. The configuration of sugar edges of adenosine and guanosine in 2′,3′-cGAMP are quite different especially in their connection by phosphate moieties. Adenosine moiety is linked by the usual 3′,5′-phosphodiester bond with the convex-free 2′-hydroxyl group, whereas the guanosine moiety is connected by the unusual 2′,5′-phosphodiester bond with the concave-free 3′-hydroxyl group (Fig. S1*B*). To accommodate these two different sugar edges of the nucleoside, helix 2 from each STING protomer adopts different conformations. The hydroxyl group of Thr-263 in helix 2 from protomer A in the G site specifically forms two hydrogen bonds with the guanine moiety, whereas only one hydrogen bond can be formed if the guanine moiety was replaced by the adenine moiety because of the absence of an extra exocyclic-amino group at the C6-position. The recognition of guanine moiety by Thr-263 will generate a steric clash if the usual 3′,5′-phosphodiester linkage with convex-free 2′-hydroxyl group presents. However, the unusual 2′,5′-phosphodiester linkage with the concave- free 3′-hydroxyl group could solve this problem

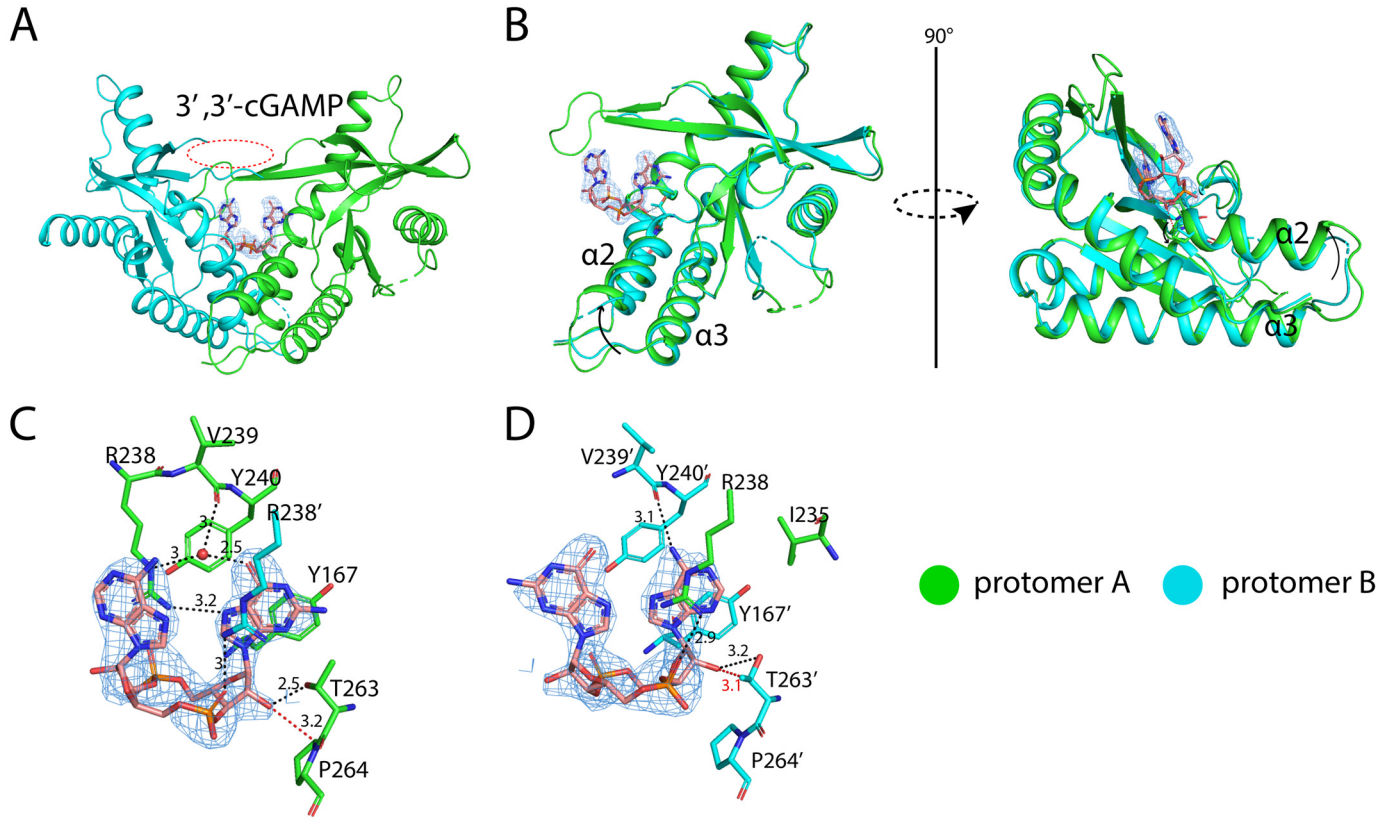

Figure 8. The structure of porcine STING^{CBD} in complex with 3′,3′-cGAMP. The *black dashed line* represents the hydrogen bond formed between ligand and protein. The values indicate the length of hydrogen bond with the unit of Å. The *red dashed line* represents the repulsive Van der Waals contact (bad contact or bump) and the values show the distance between nonhydrogen-bonding atoms. The waters are shown as *red sphere*. The ligand is shown as a *stick* model colored in *salmon*. The simulated annealing omit $F_o - F_c$ electron-density map for 3′,3′-cGAMP (*blue mesh*) is contoured at 3 σ. *A*, overall structure of porcine STING^{CBD}-3′,3′-cGAMP complex (side view). The *red dashed circle* shows the disordered lid region in protomer B. *B*, structural comparison between two protomers in porcine STING^{CBD}-3′,3′-cGAMP complex. The *arrow* indicates the tilt of α2-α3 in protomer A relative to it in protomer B. *C*, detailed interactions between Guanosine moiety of 3′,3′-cGAMP and G site of STING protein. *D*, detailed interactions between Adenosine moiety of 3′,3′-cGAMP and A site of STING protein.

properly by shifting away from the side chains of Thr-263 and Pro-264 (Fig. 5*C*). Therefore, Thr-263 and Pro-264 from protomer A in the G site form a specific recognition motif (designated as TP motif) to engage the unique sugar edge of guanosine with 2′,5′-phosphodiester linkage. However, Thr-263 in helix 2 from protomer B in the A site could not specifically recognize the sugar edge of adenosine, which lacks the exocyclic-amino group at position-C2 of the purine ring. The indirect interaction (water-mediated hydrogen bond) between Thr-263 and the N3 atom of adenine will generate enough space resolving the possible steric clashes between the convex-free 2′-hydroxyl group and Thr-263 and Pro-264 (Fig. 5*D*).

Superimposing protomer B to protomer A shows helix 2 and helix 3 in protomer A tilts upward, and the hydrophobic core undergoes rearrangement in protomer A (Fig. 6, *A–C*). The conformational changes of helix 2 and helix 3 in protomer A during ligand recognition can be considered as the movement of a lever. Helix 2 and helix 3 function as the beam, whereas Pro-264 is the turning point. The recognition of GMP(2′,5′) moiety by the TP motif will input the force at one end of the lever and result in the movement of the beam. In addition, the phosphate moiety in the 2′,5′-linkage part sticks higher than its counterpart in the 3′,5′-linkage, and therefore, the side chain of Arg-238 is bumped up by the phosphate moiety, and its χ3 dihedral angle is forced to adopt an unfavored gauche rotamer other than the anti-rotamer in protomer A, further contributing to the asymmetric conformation of the lid region (Fig. 6*D*). As described above, porcine STING using complete A site specifically recognizes AMP(3′,5′) moiety, while using incomplete G site specifically recognizes GMP(2′,5′) moiety.

Structures of porcine STING^{CBD} complex with other CDNs reveal the binding preference

As shown above, porcine STING^{CBD} adopts asymmetric conformation to bind 2′,3′-cGAMP. This prompted us to explore how porcine STING binds other more symmetric 3′,3′-CDNs. We crystallized porcine STING^{CBD} complex with bacterial second messengers, including c-di-GMP, c-di-AMP, and 3′,3′-cGAMP. All the crystals belong to the $P2_12_12_1$ space group with two molecules of STING protein per asymmetric unit. To our surprise, all the three 3′,3′-CDNs can induce porcine STING^{CBD} to adopt the similar asymmetric conformation as the 2′,3′-cGAMP does (Figs. 7–9). Besides, the c-di-AMP can induce porcine STING^{CBD} to form a much more symmetric conformation with all the lid region becoming totally visible (Fig. 10). However, the tilt of helix 2 and helix 3 in protomer A (comparing with that in protomer B) of the 3′,3′-CDN–porcine STING^{CBD} complex is not as dra-

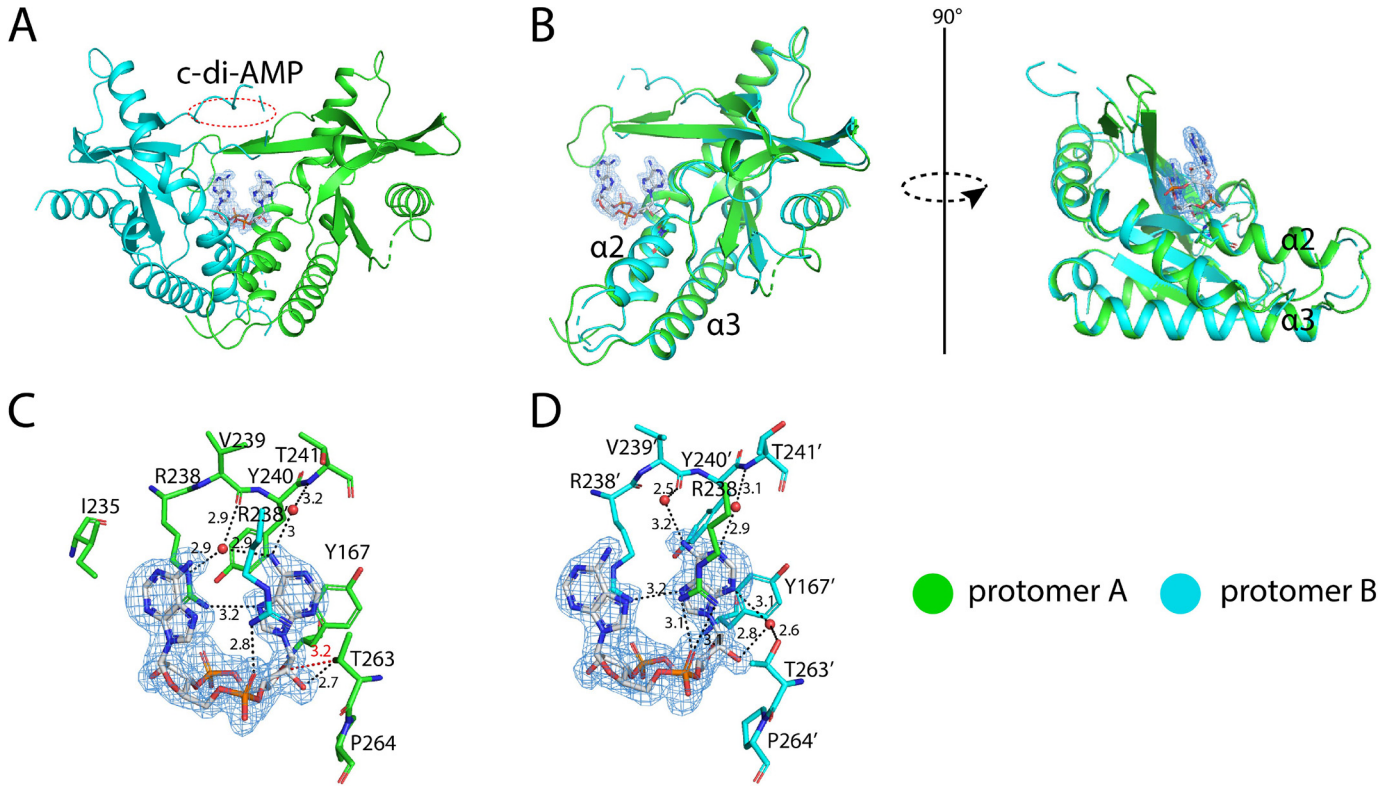

Figure 9. Structure of porcine STING^{CBD} in complex with c-di-AMP with incomplete lid region. The *black dashed line* represents the hydrogen bond formed between ligand and protein. The values indicate the length of hydrogen bond with the unit of Å. The *red dashed line* represents the repulsive van der Waals contact (bad contact or bump), and the values show the distance between nonhydrogen-bonding atoms. The waters are shown as a *red sphere*. The ligand is shown as a *stick* model colored in *silver*. The simulated annealing omit $F_o - F_c$ electron-density map for c-di-GMP (*blue mesh*) is contoured at 3 σ. *A*, overall structure of porcine STING^{CBD}–c-di-AMP complex (side view). The *red dashed circle* shows the disordered lid region in protomer B. *B*, structural comparison between two protomers in porcine STING^{CBD}–c-di-AMP complex. *C*, detailed interactions between c-di-AMP and G site of STING protein. *D*, detailed interactions between c-di-AMP and A site of STING protein.

matic as that seen in 2′3′-cGAMP–porcine STING^{CBD} complex (Figs. 7–10*B*).

In c-di-GMP–bound structure, the guanosine moiety in the A site shows unfavorable interactions with STING (Fig. 7*D*). For example, the extra-exocyclic-amino group at C2-position has bad contact with the aliphatic side chain of Ile-235; carbonyl oxygen in position-6 has bad contact with the carbonyl oxygen of Val-239; N3 nitrogen has bad contact with side chain of Tyr-167; N7 nitrogen and carbonyl oxygen in the C6-position have bad contacts with the side chain of Tyr-240; the free 2′-hydroxyl group in A site has the bad contact with the side chain of Thr-263 in protomer B. There is no hydrogen bond between Arg-238 and the N7 nitrogen in the guanine moiety within this binding pocket (supporting Table 1). These bad contacts can also be seen in the other CDN-porcine STING complexes (Figs. 8–10, *C* and *D*).

Superimposition of these five complex structures shows that overall these complexes look the same, especially for protomer B (Fig. 11*A*). The only difference in protomer A exists in α2 and α3 where it tilts more dramatically in the 2′,3′-cGAMP–STING complex than the other four CDN–STING complexes (Fig. 11*B*). As for the superimposed ligands, it clearly shows the preference for ligand binding. The unique sugar edge of GMP(2′,5′) moiety in 2′,3′-cGAMP is snugly engaged by the TP motif from protomer A in the G site, whereas the 3′,3′-CDNs are disfavored in this site because of steric clashes or the absence of hydrogen bonds (Fig. 11*C*). Similarly, the adenine-binding motif and Ile-235 selection lead to the preference of adenine in the A site. In other words, all the 3′,3′-CDNs adopting a symmetric conformation cannot fit them well in the asymmetric binding pocket resulting in a lower binding affinity complex.

Discussion

Since the identification of the CDN–STING pathway, many structural studies have revealed the binding and activation mechanism of STING by CDNs (22, 23). By superimposing porcine STING–ligand complex structure with other complex structures from human, mouse, and chicken, structural variations were observed among these STING proteins (Fig. 12*A*), although they share about 80% sequence identities (Fig. 12*B*). Except for its disordered lid region, protomer B from porcine STING is almost identical to the protomers from other species. However, protomer A from porcine STING cannot be superimposed well with its counterparts from other species. The striking difference is that the two helices (α2 and α3) in protomer A from porcine STING tilt upward, and in other species they adopt the same conformation as in protomer B. These differences make porcine STING exhibit an asymmetric pocket to engage asymmetric 2′,3′-cGAMP. There are several possible reasons why the STING-CDN complex structures from other species do not capture asymmetric conformation. As is known

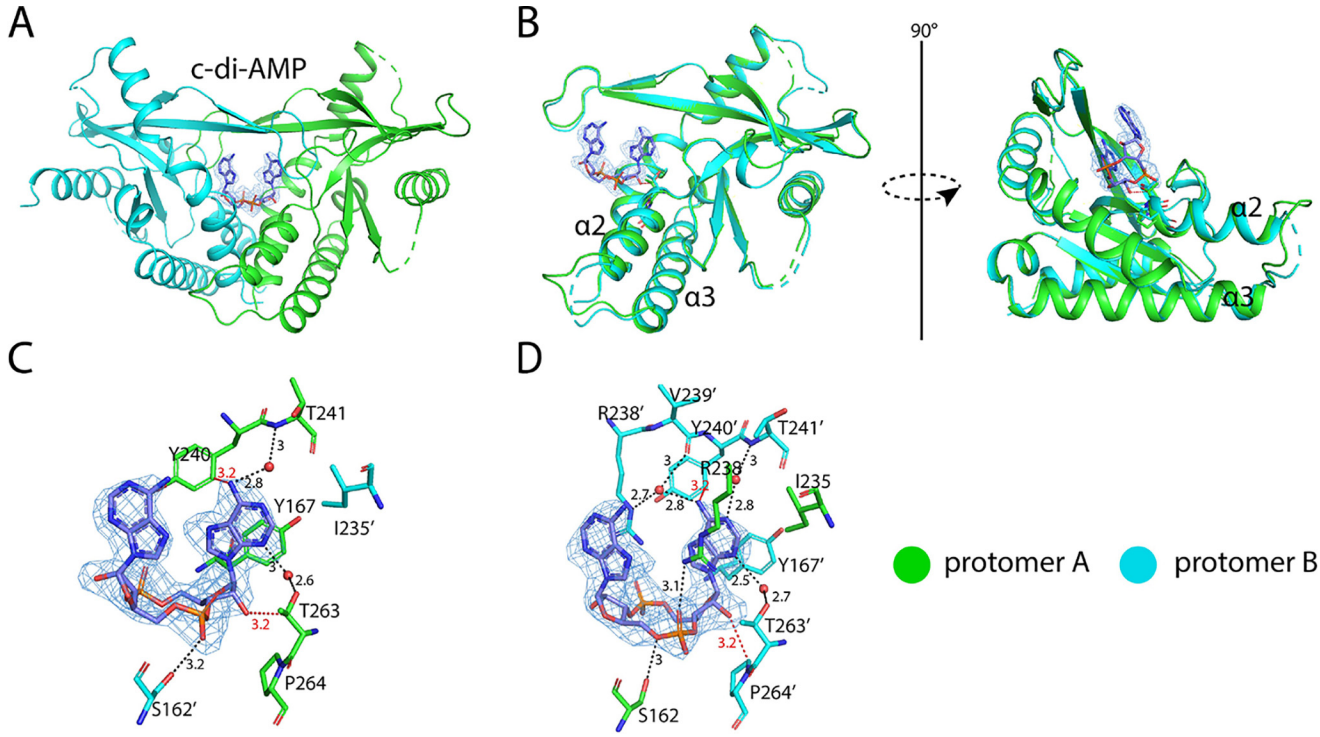

Figure 10. Structure of porcine STING^{CBD} in complex with c-di-AMP with complete lid region. The *black dashed line* represents the hydrogen bond formed between ligand and protein. The values indicate the length of hydrogen bond with the unit of Å. The *red dashed line* represents the repulsive van der Waals contact (bad contact or bump), and the values show the distance between nonhydrogen-bonding atoms. The waters are shown as a *red sphere*. The ligand is shown as a *stick* model colored in *slate blue*. The simulated annealing omit $F_o - F_c$ electron-density map for c-di-GMP (*blue mesh*) is contoured at 3 σ. *A*, overall structure of porcine STING^{CBD}–c-di-AMP complex (side view). *B*, structural comparison between two protomers in porcine STING^{CBD}–c-di-AMP complex. *C*, detailed interactions between c-di-AMP and G site of STING protein. *D*, detailed interactions between c-di-AMP and A site of STING protein.

to all, the protein crystal structure is only a snapshot of various conformers in thermodynamic equilibrium. The crystals represent the state of the global minimum free energy taking into account both natural and unspecific interactions (36). Considering that the extensive interactions occurred between the N-terminal region and the CDN-binding domain of STING (23) and only the C terminus of STING itself is included in crystallization, the unspecific interactions observed in the crystalline state of STING^{CBD} may sacrifice the natural conformation and choose the lowest-energy one. Another point is that (*e.g.* PDB code 4KSY) the crystallographic 2-fold axis passes through the dimer interface, which can average the electron density resulting in two identical protomers. As for the chicken STING–2′,3′-cGAMP complex solved by the cryo-EM method, C2 symmetry was applied during 3D focus refinement, which will make the two protomers totally the same (23).

It is difficult to explain why STING prefers the asymmetric ligand by using the complex structures solved before. Shi *et al.* (32) reported that the 2′,3′-cGAMP does not undergo large conformational change when it binds to STING and has less entropy costs leading to the highest binding affinity for 2′,3′-cGAMP. However, they ignored the contribution of protein–ligand interaction, which plays a critical role in determining the binding affinity. Although all the CDNs can induce porcine STING to form an asymmetric binding pocket, only the asymmetric 2′,3′-cGAMP can fit into this pocket well, whereas other 3′,3′-CDNs can generate constraint and suboptimal contacts, thereby limiting the interaction.

All in all, our structural investigation of porcine STING^{CBD}–CDN complexes has provided novel insight into the structural basis for ligand binding and discrimination that has implications in activation and regulation of the STING pathway.

Experimental procedures

Protein expression and purification

The cDNA encoding the porcine STING CBD domain (from 152 to 379 amino acids) was amplified and inserted into the pET-22b(+) vector (Novagen) generating the pET-22b–STING^{CBD} expression vector. The BL21(DE3) cells carrying pET-22b–STING^{CBD} vector were grown in Luria broth (LB) medium. When the A_{600} reached 0.8, the protein expression was induced by using 0.1 mM isopropyl 1-thio-β-D-galactopyranoside. After 14 h induction, the cells were collected by centrifugation (15 min, 12,000 × *g*). Then, the cell pellet was resuspended in ice-cold lysis buffer (25 mM Tris-HCl, pH 8.0, 500 mM NaCl) and lysed by sonication. The lysate was centrifuged at 30,000 × *g* for 45 min, and the supernatant was loaded onto a nickel-chelating Sepharose column (GE Healthcare) equilibrated with lysis buffer. After washing with wash buffer (25 mM Tris-HCl, pH 8.0, 300 mM NaCl, 20 mM imidazole), the bound protein was eluted by using elution buffer (25 mM Tris-HCl, pH 8.0, 100 mM NaCl, 250 mM imidazole). Then, the protein was treated with the

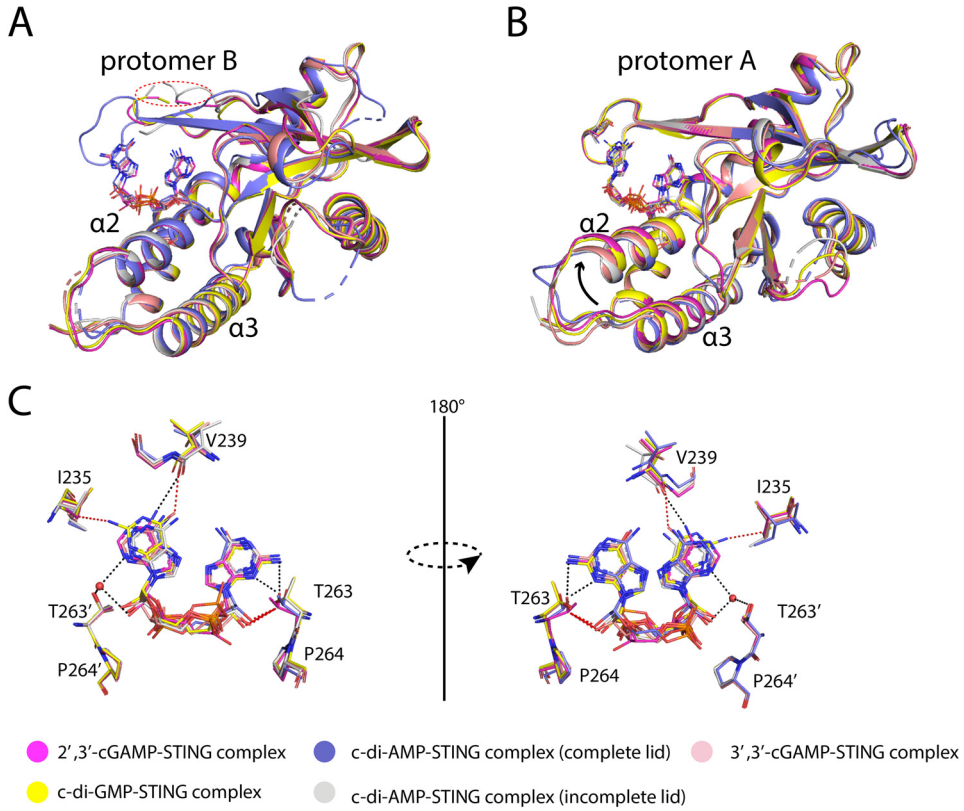

Figure 11. Structural comparison of porcine STING^{CBD}–CDNs complex. *A,* structural comparison of protomer B of porcine STING^{CBD}–CDNs complex. The lid regions of protomer B are incomplete except one of porcine STING^{CBD}–c-di-AMP complex. The *red dashed circle* shows the disordered lid region in protomer B. *B,* structural comparison of protomer A of porcine STING^{CBD}–CDN complex. The tilt of α2–α3 in 2′,3′-cGAMP is the most dramatic one. The *black arrow* indicates the upward movement of α2–α3. *C,* superimposition of CDNs shows the 2′,3′-cGAMP is the favorite ligand for STING. The *black dashed line* represents the hydrogen bond. The *red dashed line* represents the repulsive van der Waals contact (bad contact or bump).

protease trypsin in a 1:10,000 mass ratio overnight at 4 °C to remove the flexible tail region. The protease inhibitor phenylmethylsulfonyl fluoride was added to the protein solution to stop the enzymatic reaction. The protein was then applied to the Q column and eluted using a linear 160-ml gradient of 0–0.5 M NaCl. Porcine STING^{CBD} was further purified by gel-filtration chromatography by using a Superdex-200 (GE Healthcare) column equilibrated with gel-filtration buffer (10 mM Tris-HCl, pH 8.0, 100 mM NaCl). The peak was pooled and concentrated to 20 mg ml^{-1} for crystallization.

Crystallization, data collection, structure determination, and refinement

Before crystallization screening, porcine STING was mixed with 2′,3′-cGAMP and three other 3′,3′-CDNs at a 1:1.2 and 1:5 molar ratio, respectively, and incubated for 2 h at 293 K. Sitting-drop vapor-diffusion method was used for the initial screening, and the hits were optimized by using hanging-drop vapor-diffusion method at 293 K. Porcine STING^{CBD}–c-di-AMP complex can be crystallized with 3.5 M sodium formate or 1.5 M Li_2SO_4 as precipitant at 0.1 M NaOAC, pH 4.6. Porcine STING^{CBD}–3′,3′-cGAMP, c-di-GMP, and 2′,3′-cGAMP complexes were crystallized in the same condition with 1.5 M Li_2SO_4 as precipitant at 0.1 M NaOAc, pH 4.6.

The crystals were cryoprotected by 20% (v/v) glycerol and flash-frozen in liquid nitrogen before data collection. The diffraction data were collected on beamline BL17U1 at Shanghai Synchrotron Radiation Facility (SSRF). The data collected were indexed, integrated, and scaled with HKL-2000 (16).

All five complex structures were solved by the molecular replacement method with the human STING^{CBD} structure (PDB code 4F5W) as the search model. Coot (17) and PHENIX (18) were used for manual model building and refinement, respectively. The final models were deposited in the PDB with entries 6A03, 6A04, 6A05, 6A06, and 6IYF. The statistics of data collection and structure refinement are listed in Table 1. All the structure figures were rendered with PyMOL.

MST assay

MST assay was performed to measure the affinity of the purified porcine STING for CDNs with Monolith NT.115 from Nanotemper Technologies. Proteins were fluorescently labeled according to the manufacturer's protocol, and the concentration of labeled protein used for each assay was about 200 nM. A solution of unlabeled CDNs was diluted for appropriate serial concentration gradients. The samples were loaded into silica capillaries (Polymicro Technologies) after incubation at room temperature for 30 min. Measurements were performed at 293 K in buffer containing 50 mM BisTris, pH 7.6, 150 mM NaCl, and 0.05% Tween 20, by using 12% LED power and 40% MST power. The assays were repeated three times for each

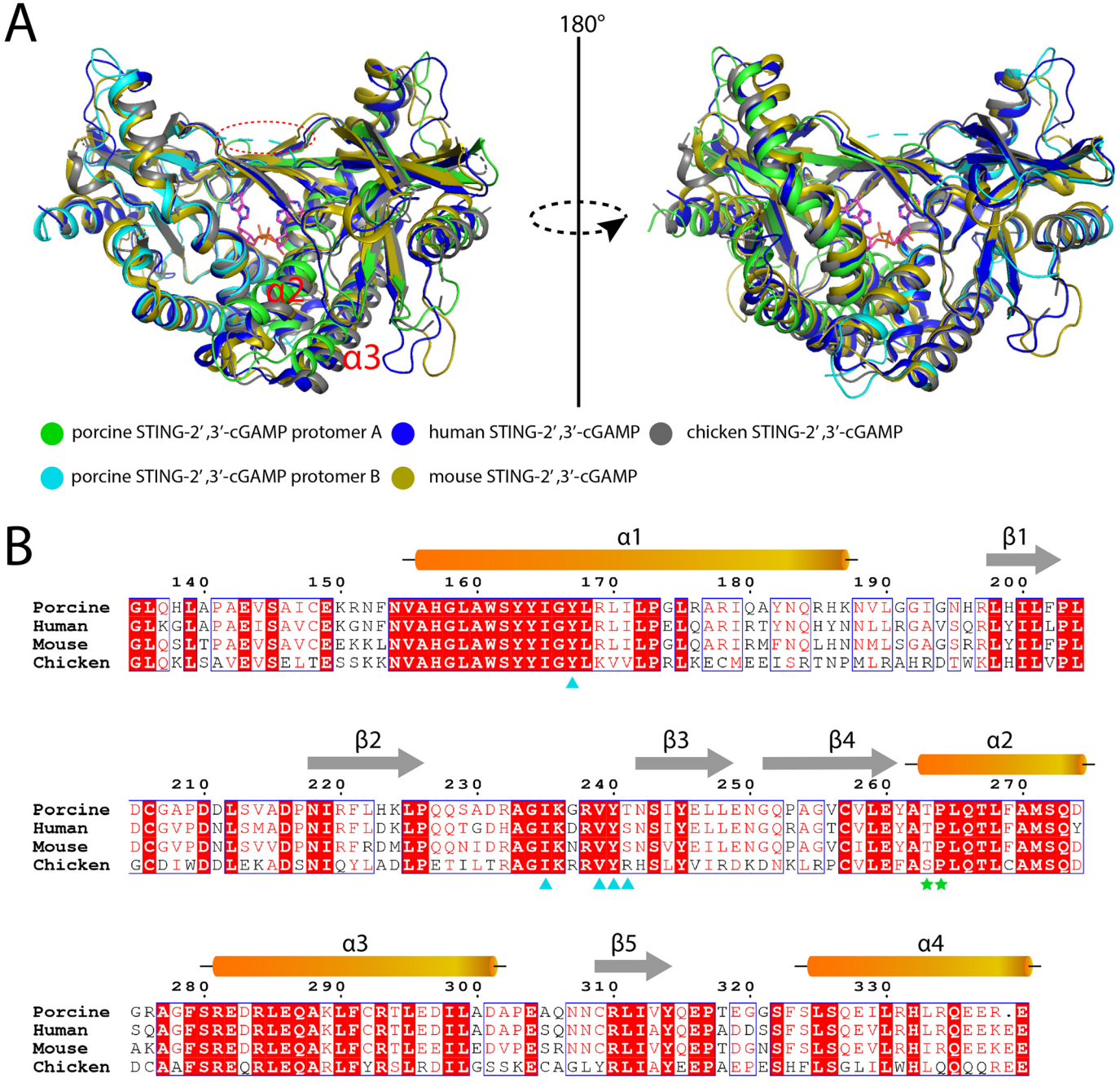

Figure 12. Structural comparison of STING^{CBD}–2′,3′-cGAMP complex from different species. *A,* protomer B except for the lid region in porcine STING is the same as protomers from other species. The *red dashed circle* shows the disordered lid region in protomer B. Protomer A in porcine STING cannot be superimposed well with protomers from other species. PDB code for human STING^{CBD}–2′,3′-cGAMP complex, 4LOH; PDB code for mouse STING^{CBD}–2′,3′-cGAMP complex, 4LOJ; PDB code for chicken STING^{CBD}–2′,3′-cGAMP complex, 6NT7. *B,* sequence alignment of human, mouse, chicken, and porcine STING^{CBD} domain. The residues in the adenine-binding motif are marked by *cyan triangles*. The residues in the TP motif are marked by *green stars*.

affinity measurement. Data analyses were performed with Nanotemper Analysis software and OriginPro 8.0 software provided by the manufacturer.

Cell-based interferon-β luciferase reporter assay

PAM, RAW264.7 or HEK293 cells were seeded in 12-well plates and grown to 80% confluence, respectively. Cells were transfected with 0.5 μg of IFN-β promoter along with 0.25 μg of pRL-TK using Lipofectamine 3000 reagent (Invitrogen). At 18 h post-transfection, PAM and RAW264.7 cells were incubated with 60 μM c-di-AMP, c-di-GMP, 3′,3′-cGAMP, or 2′,3′-cGAMP for 19 h. For HEK293 cells, 60 μM c-di-AMP, c-di-GMP, 3′,3′-cGAMP, or 2′,3′-cGAMP were transfected into cells using Lipofectamine 3000 reagent. Luciferase activities were measured using a Dual-Luciferase reporter assay kit (Promega, Madison, WI) according to the manufacturer's protocol. The values were normalized with respect to *Renilla* luciferase activities. Then, the results were expressed as relative luciferase activities, which were shown as relative fold changes compared with the mock-treated control (untransfected cells). All assays

Table 1
Data collection and refinement statistics
Each dataset was collected from a single crystal.

	STING^{CBD}–c-di-GMP complex	STING^{CBD}–c-di-AMP complex (complete lid)	STING^{CBD}–c-di-AMP complex (incomplete lid)	STING^{CBD}–3′,3′-cGAMP complex	STING^{CBD}–2′,3′-cGAMP complex
Protein Data Bank codes	6A04	6A03	6IYF	6A05	6A06
Data collection					
Wavelength (Å)	0.9798	0.9798	0.9798	0.9798	0.9798
Space group	*P 21 21 21*	*P 21 21 21*	*P 21 21 21*	*P 21 21 21*	*P 21 21 21*
Cell dimensions					
a, *b*, *c* (Å)	49.691, 63.949, 101.591	50.517, 80.459, 101.564	49.785, 65.896, 100.571	49.405, 64.741, 100.953	49.628, 63.311, 101.036
α, *β*, *γ*	90.00, 90.00, 90.00	90.00, 90.00, 90.00	90.00, 90.00, 90.00	90.00, 90.00, 90.00	90.00, 90.00, 90.00
Resolution (Å)	50.00–1.90 (1.97–1.90)[a]	50.00–2.60 (2.69–2.60)	50.00–1.76 (1.79–1.76)	50.00–2.20 (2.28–2.20)	50.00–1.80 (1.86–1.80)
R_{merge}(%)	7.8 (41.3)	13.7 (54.3)	8.0 (71.1)	8.7 (50.7)	5.5 (44.9)
$\langle I/\sigma(I)\rangle$	42.20 (6.28)	19.85 (3.87)	21.37 (1.28)	30.52 (4.59)	47.45 (5.42)
Completeness (%)	97.9 (100.0)	100.0 (100.0)	99.1 (84.1)	100.0 (100.0)	99.2 (99.0)
Redundancy	6.6 (6.9)	7.1 (7.3)	7.1 (6.1)	6.9 (6.9)	7.0 (7.0)
Refinement					
No. of reflections	25,597	13,319	33,277	16,950	30,287
R_{work}/R_{free} (%)	20.21/24.96	20.00/25.72	19.36/24.21	22.15/27.35	17.53/21.99
No. of atoms					
Protein	2910	2841	2795	2921	2929
Ligand	46	44	44	45	45
Water	151	76	136	37	214
B-factors (Å^2)					
Protein	39.24	34.74	31.60	47.39	31.20
Ligand	33.53	28.79	30.05	41.84	22.92
Water	38.47	32.04	34.75	35.63	34.59
Root mean square deviation					
Bond lengths (Å)	0.007	0.003	0.011	0.008	0.006
Bond angles (°)	0.888	0.700	1.255	1.252	0.857
Ramachandran plot					
Favored (%)	96.97	94.99	97.46	94.6	96.69
Allowed (%)	3.03	4.72	2.54	5.4	3.31
Disallowed (%)	0	0.29	0	0	0

[a] Values in parentheses are for highest-resolution shell.

were repeated at least three times, with each experiment performed in triplicate.

Author contributions—X. C., F. L., and G. S. formal analysis; X. C., Z. Y., Y. D., B. Wu, D. L., X. W., Y. Z., B. Wei, J. L., J. Wu, J. Wang, and J. Q. investigation; X. C., Z. Y., Y. D., B. Wu, D. L., X. W., Y. Z., J. Q., and G. S. methodology; X. C., Y. D., F. L., J. Q., and L. G. writing-review and editing; Z. Y. and G. S. writing-original draft; Y. D. and L. G. funding acquisition; S. X. visualization; J. Wang, J. Q., and L. G. supervision; J. Q. and G. S. conceptualization; G. S. data curation; G. S. validation.

Acknowledgments—We thank the staff of beamlines BL17U1 and BL19U at the Shanghai Synchrotron Radiation Facility (SSRF) for their support in the data collection. We also thank Dr. Xuewu Zhang for critical reading and editing of this manuscript.

References

1. Pandey, S., Kawai, T., and Akira, S. (2014) Microbial sensing by Toll-like receptors and intracellular nucleic acid sensors. *Cold Spring Harb. Perspect. Biol.* **7,** a016246 CrossRef Medline
2. Kumar, H., Kawai, T., and Akira, S. (2011) Pathogen recognition by the innate immune system. *Int. Rev. Immunol.* **30,** 16–34 CrossRef Medline
3. Walsh, D., McCarthy, J., O'Driscoll, C., and Melgar, S. (2013) Pattern recognition receptors–molecular orchestrators of inflammation in inflammatory bowel disease. *Cytokine Growth Factor Rev.* **24,** 91–104 CrossRef Medline
4. Takeuchi, O., and Akira, S. (2010) Pattern recognition receptors and inflammation. *Cell* **140,** 805–820 CrossRef Medline
5. Barbalat, R., Ewald, S. E., Mouchess, M. L., and Barton, G. M. (2011) Nucleic acid recognition by the innate immune system. *Annu. Rev. Immunol.* **29,** 185–214 CrossRef Medline
6. Wu, J., and Chen, Z. J. (2014) Innate immune sensing and signaling of cytosolic nucleic acids. *Annu. Rev. Immunol.* **32,** 461–488 CrossRef Medline
7. Zhong, B., Yang, Y., Li, S., Wang, Y. Y., Li, Y., Diao, F., Lei, C., He, X., Zhang, L., Tien, P., and Shu, H. B. (2008) The adaptor protein MITA links virus-sensing receptors to IRF3 transcription factor activation. *Immunity* **29,** 538–550 CrossRef Medline
8. Zhong, B., Zhang, L., Lei, C., Li, Y., Mao, A. P., Yang, Y., Wang, Y. Y., Zhang, X. L., and Shu, H. B. (2009) The ubiquitin ligase RNF5 regulates antiviral responses by mediating degradation of the adaptor protein MITA. *Immunity* **30,** 397–407 CrossRef Medline
9. Jin, L., Waterman, P. M., Jonscher, K. R., Short, C. M., Reisdorph, N. A., and Cambier, J. C. (2008) MPYS, a novel membrane tetraspanner, is associated with major histocompatibility complex class II and mediates transduction of apoptotic signals. *Mol. Cell. Biol.* **28,** 5014–5026 CrossRef Medline
10. Sun, W., Li, Y., Chen, L., Chen, H., You, F., Zhou, X., Zhou, Y., Zhai, Z., Chen, D., and Jiang, Z. (2009) ERIS, an endoplasmic reticulum IFN stimulator, activates innate immune signaling through dimerization. *Proc. Natl. Acad. Sci. U.S.A.* **106,** 8653–8658 CrossRef Medline
11. Wu, J., Sun, L., Chen, X., Du, F., Shi, H., Chen, C., and Chen, Z. J. (2013) Cyclic GMP-AMP is an endogenous second messenger in innate immune signaling by cytosolic DNA. *Science* **339,** 826–830 CrossRef Medline
12. Saitoh, T., Fujita, N., Hayashi, T., Takahara, K., Satoh, T., Lee, H., Matsunaga, K., Kageyama, S., Omori, H., Noda, T., Yamamoto, N., Kawai, T., Ishii, K., Takeuchi, O., Yoshimori, T., and Akira, S. (2009) Atg9a controls dsDNA-driven dynamic translocation of STING and the innate immune response. *Proc. Natl. Acad. Sci. U.S.A.* **106,** 20842–20846 CrossRef Medline
13. Ishikawa, H., Ma, Z., and Barber, G. N. (2009) STING regulates intracellular DNA-mediated, type I interferon-dependent innate immunity. *Nature* **461,** 788–792 CrossRef Medline
14. Dobbs, N., Burnaevskiy, N., Chen, D., Gonugunta, V. K., Alto, N. M., and Yan, N. (2015) STING activation by translocation from the ER is associ-

ated with infection and autoinflammatory disease. *Cell Host Microbe* **18,** 157–168 CrossRef Medline
15. Tanaka, Y., and Chen, Z. J. (2012) STING specifies IRF3 phosphorylation by TBK1 in the cytosolic DNA signaling pathway. *Sci. Signal.* **5,** ra20 CrossRef Medline
16. Liu, S., Cai, X., Wu, J., Cong, Q., Chen, X., Li, T., Du, F., Ren, J., Wu, Y. T., Grishin, N. V., and Chen, Z. J. (2015) Phosphorylation of innate immune adaptor proteins MAVS, STING, and TRIF induces IRF3 activation. *Science* **347,** aaa2630 CrossRef Medline
17. Burdette, D. L., Monroe, K. M., Sotelo-Troha, K., Iwig, J. S., Eckert, B., Hyodo, M., Hayakawa, Y., and Vance, R. E. (2011) STING is a direct innate immune sensor of cyclic di-GMP. *Nature* **478,** 515–518 CrossRef Medline
18. Jenal, U., Reinders, A., and Lori, C. (2017) Cyclic di-GMP: second messenger extraordinaire. *Nat. Rev. Microbiol.* **15,** 271–284 CrossRef Medline
19. Davies, B. W., Bogard, R. W., Young, T. S., and Mekalanos, J. J. (2012) Coordinated regulation of accessory genetic elements produces cyclic di-nucleotides for *V. cholerae* virulence. *Cell* **149,** 358–370 CrossRef Medline
20. Gao, P., Ascano, M., Zillinger, T., Wang, W., Dai, P., Serganov, A. A., Gaffney, B. L., Shuman, S., Jones, R. A., Deng, L., Hartmann, G., Barchet, W., Tuschl, T., and Patel, D. J. (2013) Structure–function analysis of STING activation by c[G(2′,5′)pA(3′,5′)p] and targeting by antiviral DMXAA. *Cell* **154,** 748–762 CrossRef Medline
21. Zhang, X., Shi, H., Wu, J., Zhang, X., Sun, L., Chen, C., and Chen, Z. J. (2013) Cyclic GMP-AMP containing mixed phosphodiester linkages is an endogenous high-affinity ligand for STING. *Mol. Cell* **51,** 226–235 CrossRef Medline
22. Kato, K., Omura, H., Ishitani, R., and Nureki, O. (2017) Cyclic GMP-AMP as an endogenous second messenger in innate immune signaling by cytosolic DNA. *Annu. Rev. Biochem.* **86,** 541–566 CrossRef Medline
23. Shang, G., Zhang, C., Chen, Z. J., Bai, X. C., and Zhang, X. (2019) Cryo-EM structures of STING reveal its mechanism of activation by cyclic GMP-AMP. *Nature* **567,** 389–393 CrossRef Medline
24. Ouyang, S., Song, X., Wang, Y., Ru, H., Shaw, N., Jiang, Y., Niu, F., Zhu, Y., Qiu, W., Parvatiyar, K., Li, Y., Zhang, R., Cheng, G., and Liu, Z. J. (2012) Structural analysis of the STING adaptor protein reveals a hydrophobic dimer interface and mode of cyclic di-GMP binding. *Immunity* **36,** 1073–1086 CrossRef Medline
25. Shu, C., Yi, G., Watts, T., Kao, C. C., and Li, P. (2012) Structure of STING bound to cyclic di-GMP reveals the mechanism of cyclic dinucleotide recognition by the immune system. *Nat. Struct. Mol. Biol.* **19,** 722–724 CrossRef Medline
26. Huang, Y. H., Liu, X. Y., Du, X. X., Jiang, Z. F., and Su, X. D. (2012) The structural basis for the sensing and binding of cyclic di-GMP by STING. *Nat. Struct. Mol. Biol.* **19,** 728–730 CrossRef Medline
27. Shang, G., Zhu, D., Li, N., Zhang, J., Zhu, C., Lu, D., Liu, C., Yu, Q., Zhao, Y., Xu, S., and Gu, L. (2012) Crystal structures of STING protein reveal basis for recognition of cyclic di-GMP. *Nat. Struct. Mol. Biol.* **19,** 725–727 CrossRef Medline
28. Yin, Q., Tian, Y., Kabaleeswaran, V., Jiang, X., Tu, D., Eck, M. J., Chen, Z. J., and Wu, H. (2012) Cyclic di-GMP sensing via the innate immune signaling protein STING. *Mol. Cell* **46,** 735–745 CrossRef Medline
29. Chin, K. H., Tu, Z. L., Su, Y. C., Yu, Y. J., Chen, H. C., Lo, Y. C., Chen, C. P., Barber, G. N., Chuah, M. L., Liang, Z. X., and Chou, S. H. (2013) Novel c-di-GMP recognition modes of the mouse innate immune adaptor protein STING. *Acta Crystallogr. D Biol. Crystallogr.* **69,** 352–366 CrossRef Medline
30. Zhang, H., Han, M. J., Tao, J., Ye, Z. Y., Du, X. X., Deng, M. J., Zhang, X. Y., Li, L. F., Jiang, Z. F., and Su, X. D. (2015) Rat and human STINGs profile similarly towards anticancer/antiviral compounds. *Sci. Rep.* **5,** 18035 CrossRef Medline
31. Kranzusch, P. J., Wilson, S. C., Lee, A. S., Berger, J. M., Doudna, J. A., and Vance, R. E. (2015) Ancient origin of cGAS-STING reveals mechanism of universal 2′,3′-cGAMP signaling. *Mol. Cell* **59,** 891–903 CrossRef Medline
32. Shi, H., Wu, J., Chen, Z. J., and Chen, C. (2015) Molecular basis for the specific recognition of the metazoan cyclic GMP-AMP by the innate immune adaptor protein STING. *Proc. Natl. Acad. Sci. U.S.A.* **112,** 8947–8952 CrossRef Medline
33. Denessiouk, K. A., Rantanen, V. V., and Johnson, M. S. (2001) Adenine recognition: a motif present in ATP-, CoA-, NAD-, NADP-, and FAD-dependent proteins. *Proteins* **44,** 282–291 CrossRef Medline
34. Stefl, R., Oberstrass, F. C., Hood, J. L., Jourdan, M., Zimmermann, M., Skrisovska, L., Maris, C., Peng, L., Hofr, C., Emeson, R. B., and Allain, F. H. (2010) The solution structure of the ADAR2 dsRBM–RNA complex reveals a sequence-specific readout of the minor groove. *Cell* **143,** 225–237 CrossRef Medline
35. Masliah, G., Barraud, P., and Allain, F. H. (2013) RNA recognition by double-stranded RNA binding domains: a matter of shape and sequence. *Cell. Mol. Life Sci.* **70,** 1875–1895CrossRef Medline
36. Krissinel, E. (2010) Crystal contacts as nature's docking solutions. *J. Comput. Chem.* **31,** 133–143 CrossRef Medline